

## Organic long persistent luminescence wood-based materials

Xixi Piao, Zhengwen Ning, Qingxin He, Yue Zhang, Tengyue Wang, Guangming Wang,  
Kaka Zhang\*

*State Key Laboratory of Organometallic Chemistry and Shanghai Hongkong Joint Laboratory in Chemical Synthesis, Key Laboratory of Synthetic and Self-Assembly Chemistry for Organic Functional Molecules, Shanghai Institute of Organic Chemistry, University of Chinese Academy of Sciences, Chinese Academy of Sciences, 345 Lingling Road, Shanghai 200032, People's Republic of China*



### ARTICLE INFO

**Keywords:**  
Organic long persistent luminescence  
Transparent wood  
Wood-based materials  
Pyrylium salt

### ABSTRACT

As an emerging environmentally friendly material, the biggest advantage of wood-based materials lies in its renewability and green sustainability, which helps reduce the ecological impact on the environment. There have been some studies on room-temperature phosphorescent wood-based materials nowadays, but no one has explored them in the field of organic long persistent luminescence (OLPL). Here, we report the high-performance organic afterglow observed in the pyrylium salt (Pyr) induced photopolymerization system, and combine it with transparent wood to prepare unprecedented OLPL materials with emission maxima at approximately 596 nm and lasting for more than 1 h. The transparent wood matrix can provide a rigid environment for the Pyr system and act as an oxygen barrier, inhibiting non-radiative decay and oxygen quenching. At the same time, the transparent wood also has good transparency and other characteristics, which can be considered one of the most promising alternative materials in the future. We have also prepared OLPL wood coatings, adhesives, and wood-plastic composites. The combination of various wood-based materials and luminescent technology not only enhances aesthetics and practicality of wood products, but also promotes technological innovation and development in the fields of anti-counterfeiting and data encryption, green building materials, and emergency lighting.

### 1. Introduction

In recent years, the development of green materials with functional properties using natural and renewable resources has made huge contributions toward sustainable development [1]. Wood is a traditional natural green structural material with unique characteristics, such as low density, high modulus, high strength, and low thermal conductivity [2–6]. Due to its porous characteristics, it has been ubiquitous in applications ranging from construction, transportation, and various material fabrications for thousands of years [7–9]. Wood is mainly composed of cellulose, hemicellulose, and lignin, these bio-based macromolecules contain a series of different functional groups, and the functionalization of wood has been achieved through various physical, chemical, and processing treatments [10–13]. Among them, transparent wood (TW) prepared from wood exhibits excellent optical properties and has been widely used in the preparation of optoelectronic devices and building materials [14,15]. For example, Hu and coworkers [16] prepared a novel type of stretchable aesthetic transparent wood (ATW) with good optical and mechanical properties, making ATW a promising

candidate for green building materials with additional aesthetic functions. Fu et al. infiltrated quantum dots (CdSe/ZnS) into wood to generate samples with isotropic light scattering and luminescence, which could be used in the design of indoor lamps [17]. By changing the types of quantum dots in the fabrication process, more colors of light can be obtained, which is a potential lighting application of TW [18,19]. Therefore, TW materials have been widely used due to their abundance, renewability, stability, and sustainability [20–23]. Especially in optoelectronic applications, TW retains the unique hierarchical structure of wood, providing a rigid environment, dense hydrogen-bonding sites, and an excellent oxygen barrier to suppress the non-radiative deactivation of triplet excitons [24,25]. However, although there are some reports on room-temperature phosphorescent wood and luminescent TW exhibiting promising applications in anti-counterfeiting, data encryption, sensing and lighting [13,20,23,25], afterglow duration and color tunability are still very limited, and there are no reports on the preparation of organic long persistent luminescent TW.

Moreover, apart from afterglow transparent wood, there is a significant lack of wooden materials that combine natural aesthetics with

\* Corresponding author.

E-mail address: [zhangkaka@sioc.ac.cn](mailto:zhangkaka@sioc.ac.cn) (K. Zhang).

unique luminescent functionalities in other wood-based systems [26,27]. For instance, long afterglow wood coatings and adhesives not only possess their inherent coating and adhesive properties but also exhibit excellent visual effects and practical value [28,29]. These materials can be widely applied in architectural decoration, furniture, and toys, enhancing both functionality and aesthetic appeal while improving visibility and safety in nighttime or low-light conditions [30,31]. Also, long-afterglow wood-plastic composites can emit a soft glow in the dark, particularly useful as markers for buildings, landscapes, and emergency pathways in parks, adding a special visual beauty [32]. However, the current methods for preparing room-temperature phosphorescent wood-based materials typically involve introducing small amounts of afterglow components into existing materials. This approach has several drawbacks, including low efficiency, short afterglow duration, uneven distribution of afterglow components, and complex preparation processes [29–31]. Therefore, the development of uniformly stable long afterglow wood coatings, adhesives, and wood-plastic composites holds great promise for various practical applications. To date, there have been no reports of organic long persistent luminescent wood-based products.

Room-temperature phosphorescence (RTP) and organic long persistent luminescence (OLPL) materials are a class of unique luminescent materials with much longer emission lifetimes than fluorescent materials [33–35]. Recent studies have shown that RTP and organic long persistent luminescent materials have wide applications in oxygen sensing, mapping, anti-counterfeiting, data encryption, background-free bioimaging, and time-gated optical sensing. [36–43] The long-lifetime properties of RTP and afterglow materials originate from the triplet excited states, which are not easily formed and are prone to oxygen quenching or non-radiative deactivation due to spin-forbidden transition and weak spin-orbit coupling [44–47]. Pioneering studies in this field have demonstrated that the afterglow quantum efficiency in organic systems can be greatly improved by rational molecular design, aggregation control of molecules, and supramolecular assembly strategies [48–62]. For example, in some reported studies, heavy-atom effects and  $n-\pi^*$  transitions are often used to enhance the intersystem crossing and phosphorescence decay, thus improving the organic afterglow efficiency [33–53]. However, the heavy-atom effect usually largely enhances the phosphorescence decay, thus shortening the phosphorescence lifetime [50]. The involvement of  $n-\pi^*$  transitions in the organic  $T_1$  state (where  $T_1$  represents the lowest triplet excited state) also accelerates the phosphorescence decay, reducing the phosphorescence lifetime [39,51–53]. In donor–acceptor systems, the appropriate combination of organic molecules can generate OLPL lasting for several hours through photo-induced charge separation (CS) and subsequent

delayed charge recombination [55,63]. Recent studies have shown that such donor–acceptor systems can maintain their OLPL properties even when exposed to ambient conditions or dispersed in aqueous media [38–43,64–68]. This binary design strategy allows for the flexible selection of luminescent dopants and organic matrices to construct afterglow materials with various structures and compositions [69–74].

Herein, we report the fabrication of high-performance organic afterglow systems by pyrylium salt (Pyr) induced photopolymerization systems of methyl methacrylate (MMA) and 9-vinylcarbazole (NVK) in a wood frame, exhibiting unprecedented OLPL transparent wood for the first time (Fig. 1). In-depth studies reveal that intermolecular charge transfer (CT) is responsible for the formation of the charge-separated state in the Pyr-PVK donor–acceptor pairs. Equally important is the role of PMMA-wood as a matrix in suppressing non-radiative decay and oxygen quenching, which is crucial for achieving high-performance OLPL. Furthermore, by coating the pyrylium salt-polymer system onto wood, we have developed a novel functional wood coating with long-lasting afterglow properties. We have also explored its use as a wood adhesive to replace formaldehyde-based adhesives, demonstrating promising application potential. Finally, by incorporating 10 % wood flour into the pyrylium salt-polymer system and curing it, we have produced a unique wood-plastic composite material that combines the fundamental characteristics of wood with the distinctive attributes of the luminescent material.

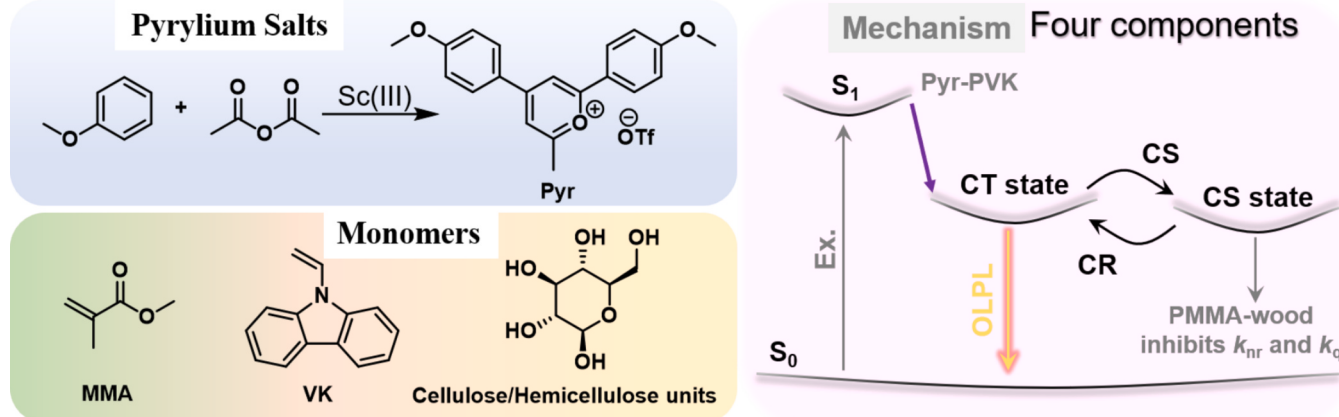
## 2. Material and methods

### 2.1. Cascade synthesis of 2,4-bis(4-methoxyphenyl)-6-methylpyrylium triflate (Pyr)

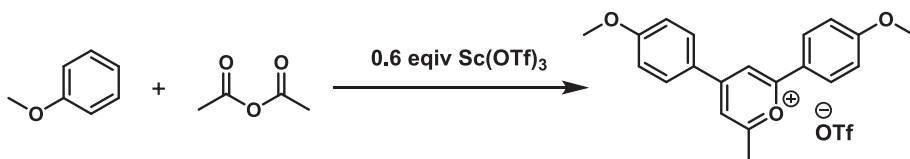
Anisole (0.100 mL, 0.92 mmol), scandium(III) triflate (55.1 mg, 0.092 mmol) and acetic anhydride (0.435 mL, 4.60 mmol) were mixed in a round bottom flask. The reaction was performed at 135 °C for 6 h. After cooling, the reaction mixture was poured into 20 mL diethyl ether, leading to the formation of precipitates (Scheme 1). After filtration, the precipitates were washed with diethyl ether, and then recrystallized twice in acetic acid/diethyl ether. Red crystals were obtained, washed with diethyl ether and dried under vacuum to give an isolation yield of 30 %. Single crystal was achieved via diethyl ether diffusion into acetonitrile solution of Pyr. The synthesis was carried out using the methods in previous study [68,75].

### 2.2. Preparation of afterglow materials in Pyr-PVK system

For the preparation of 0.05 %-Pyr-PVK materials, Pyr and NVK were



**Fig. 1.** Synthesis of Pyr and chemical structures of monomers. In the poly(vinyl carbazole) (PVK) system, the lower-lying intermolecular CT state of the PVK donor and Pyr acceptor blocks the population of Pyr's  $T_1$  states, leading to CS states under excitation. PMMA-wood matrix suppresses non-radiative decay and oxygen quenching, ensuring the emergence of OLPL.

**Scheme 1.** Synthesis of Pyr.

mixed at a weight ratio of 1/2000 in a 1 mL sample bottle through solution casting or melt casting. Within 1 min 365 nm UV LED lamp ( $160 \text{ mW/cm}^2$ ) irradiation, 0.05 %Pyr-PVK materials that exhibit orange-red afterglow with organic long persistent luminescence (OLPL) were obtained.

### 2.3. Preparation of Pyr-PMMA afterglow materials

For the preparation of 0.01 %Pyr-PMMA, 2 mL MMA and 0.2 mg Pyr were added into a 3 mL sample bottle. Then 40  $\mu\text{L}$  2-hydroxy-2-methylpropiophenon was added into the Pyr/MMA solution. After 10 min 365 nm UV LED lamp ( $160 \text{ mW/cm}^2$ ) irradiation, a glass-like object that show afterglow properties was obtained. The obtained 0.01 %Pyr-PMMA was further dissolved in 1 mL dichloromethane to better distribute Pyr in PMMA. After solvent evaporating, 0.01 %Pyr-PMMA that show sky-blue afterglow properties were obtained. The other afterglow materials in this paper with different doping concentrations were prepared through similar processes.

### 2.4. Preparation of Pyr-PVK-PMMA three-component afterglow materials

For the preparation of 0.1 %Pyr-PVK-PMMA, firstly, 1 mg Pyr and 200 mg NVK were mixed in a 3 mL sample bottle through solution casting or melt casting. Secondly, 1 mL of MMA was added to dissolve Pyr and NVK to better distribute them in MMA. Then 20  $\mu\text{L}$  2-hydroxy-2-methylpropiophenon was added into the system. The three-component organic long afterglow system of Pyr-PVK-PMMA can be obtained by curing it for 10 min under 365 nm ultraviolet radiation ( $160 \text{ mW/cm}^2$ ).

### 2.5. Preparation of OLPL transparent wood materials

Balsa wood was delignified by using 2 wt% NaClO<sub>2</sub> in CH<sub>3</sub>COOH (pH = 4.6) at 80 °C. The reaction lasted for about 4 h until the wood became totally white. The delignified wood was bleached in H<sub>2</sub>O<sub>2</sub> (30 %) solution at 90 °C for 1 h. The treated samples were washed with ultrapure water to remove the chemical residue. Then, delignified balsa wood chips were stored in ethanol and acetone solvents to maintain the rigidity of its cellulose skeleton. Then, in the preparation process of three-component prepolymer solution, the dried bleached wood was immersed in the solution and then placed in a vacuum drying oven about 1 h, where the mixture solution was filled into the bleached wood. Finally, after 10 min of 365 nm UV curing ( $160 \text{ mW/cm}^2$ ), OLPL transparent wood was obtained.

### 2.6. Preparation of OLPL wood coatings, adhesive and wood-plastic materials

The three-component prepolymer solution of 0.1 %Pyr-NVK-MMA was evenly applied on the surface of balsa wood. After curing for 10 min under 365 nm UV light ( $160 \text{ mW/cm}^2$ ), OLPL wood coating was obtained, and the thickness of the coating was measured. In a two-component material of 200 mg 0.1 %Pyr-NVK, 400 mg of UV curable resin glue (mainly composed of PMMA and photoinitiator) was added and mixed evenly by ultrasound. The adhesive was applied to a wood board at a dosage of 200 g/m<sup>2</sup> and cured by 365 nm UV light ( $160 \text{ mW/cm}^2$ ) to obtain OLPL wood adhesive. In a 600 mg three-component 0.1 %Pyr-NVK-MMA system, 10 % wood powder and 2 % photoinitiator

were added, poured into a mold, and cured by 365 nm UV irradiation ( $160 \text{ mW/cm}^2$ ) to obtain OLPL wood-plastic composites.

## 3. Results and discussion

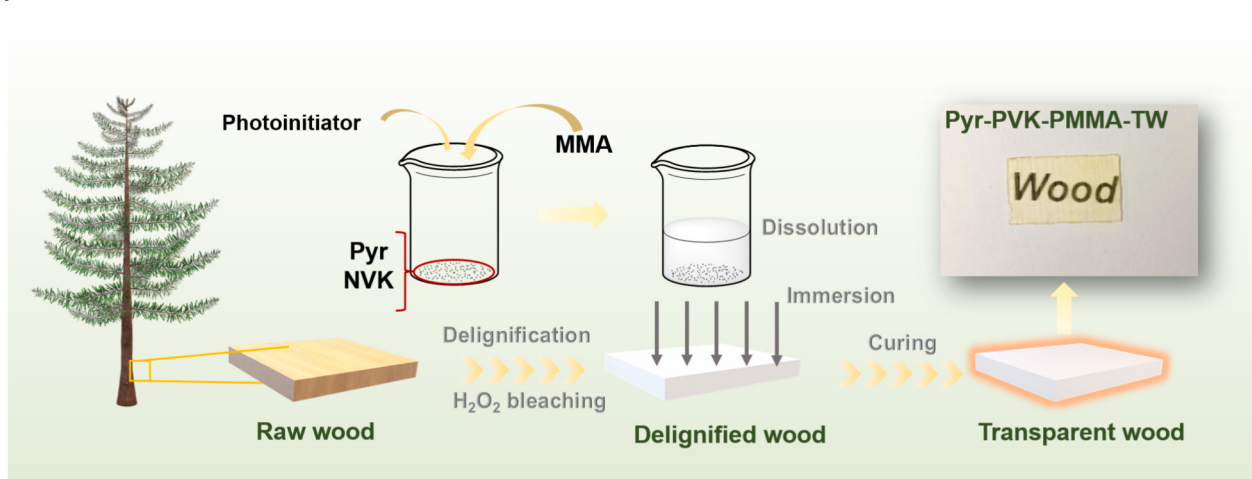
### 3.1. Pyr-PVK-PMMA-TW photophysical properties

Pyr was synthesized via a cascade reaction developed by us (Fig. 1) and a series of characterizations for Pyr were carried out (Figs. S1–S7) [68]. It exhibits an intense intramolecular charge transfer absorption band at 449 nm and bright green emission centered at 499 nm in dichloromethane with 90.7 % of photoluminescence quantum yield, 3.32 ns of fluorescence lifetime,  $33800 \text{ M}^{-1}\text{cm}^{-1}$  of molar absorption coefficient and a HOMO energy level of  $-6.53 \text{ eV}$  and a LUMO energy level of  $-3.95 \text{ eV}$  (Table S1). The intramolecular charge transfer character of Pyr in the S<sub>1</sub> state was calculated by TD-DFT. Based on our previous research, PMMA can be used as a matrix to design high-performance organic phosphorescent systems, providing beneficial assistance for their applications [76–78]. The transparent wood prepared from the combination of wood and PMMA has practical value. Therefore, we prepared four-component transparent wood materials using Pyr, NVK, PMMA, and wood according to the process shown in Fig. 2A. Here photopolymerization is selected because of its advantage of rapid curing, energy-saving and environmentally friendly, precise spatial/temporal control property. Surprisingly, it has been found that the resultant system exhibited a long orange afterglow (Fig. 2B). The steady-state emission spectrum of Pyr-PVK-PMMA-TW materials shows emission band at 596 nm, and the delayed emission (delayed 1 ms) band is also at 596 nm (Fig. 2C, D). The delayed emission intensity at room temperature (excited at 433 nm) follows power-law decay (Fig. 2E, F) with hour-long durations. The materials can also be excited by a sunlight simulator lamp (Fig. S8). Such long afterglow duration originates from Pyr-PVK luminescence center (*vide infra*), while PMMA-wood protect organic long-lived excitons and radical intermediates from nonradiative decay and oxygen quenching. PMMA's glassy microenvironment can restrict intramolecular motion of organic long-lived excitons. The high crystallinity of cellulose fibrils and abundant hydrogen bonding within wood component would suppress oxygen diffusion in the afterglow system.

### 3.2. Morphology and properties of Pyr-PVK-PMMA-TW

For the morphology of Pyr-PVK-PMMA-TW materials, SEM observation shows the filled and unfilled structures of wood in both vertical (Fig. 3A, B) and horizontal directions (Fig. 3C, D), ensuring that the wood is well infiltrated. In the FT-IR spectra, the distinct band observed at  $1632 \text{ cm}^{-1}$  precisely represents the skeletal vibration of the benzene ring (C=C stretching vibration) of lignin, which the strength of this area will be greatly reduced after delignification treatment. The characteristic of methoxy groups in lignin is also weakened at  $890 \text{ cm}^{-1}$  due to the stretching vibration of C–O in O–CH<sub>3</sub> after lignin removal [79]. In PMMA,  $1726 \text{ cm}^{-1}$  is one of the characteristic peaks caused by the stretching vibration of C=O in the ester group (–COO–), and there is a C–O–C stretching vibration at  $1150 \text{ cm}^{-1}$ , which these peaks also appear in the four-component materials (Fig. 3E) [80]. In addition, the appearance of the characteristic peak of the stretching vibration peak of ether bond (C–O–C) in Pyr at  $1180 \text{ cm}^{-1}$  and the characteristic peak of

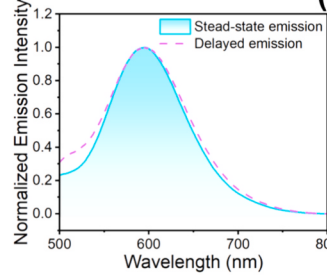
(A)



(B)



(C)



10 min

30 min

During time

(D)

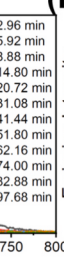
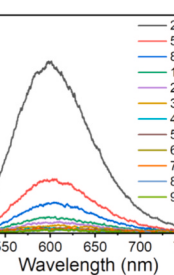
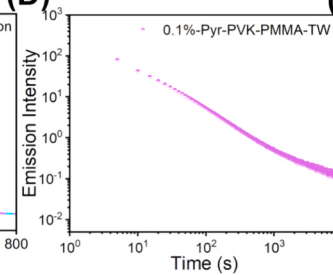


**Fig. 2.** (A) Schematic illustration of the preparation of OLPL transparent wood. (B) Photographs of 0.1 %Pyr-PVK-PMMA-TW materials under UV lamp and after removal of the excitation sources. (C) Room-temperature steady-state emission and delayed emission (1 ms delay) spectra of 0.1 %Pyr-PVK-PMMA-TW materials excited at 433 nm. (D) Room-temperature emission decay of 0.1 %Pyr-PVK-PMMA-TW materials monitored at 596 nm. (E) OLPL spectra of the 0.1 %Pyr-PVK-PMMA-TW materials as a function of delay times excited at 433 nm. (F) A logarithmic plot of the OLPL decay profile of 0.1 %Pyr-PVK-PMMA-TW materials monitored at a peak wavelength of 596 nm.

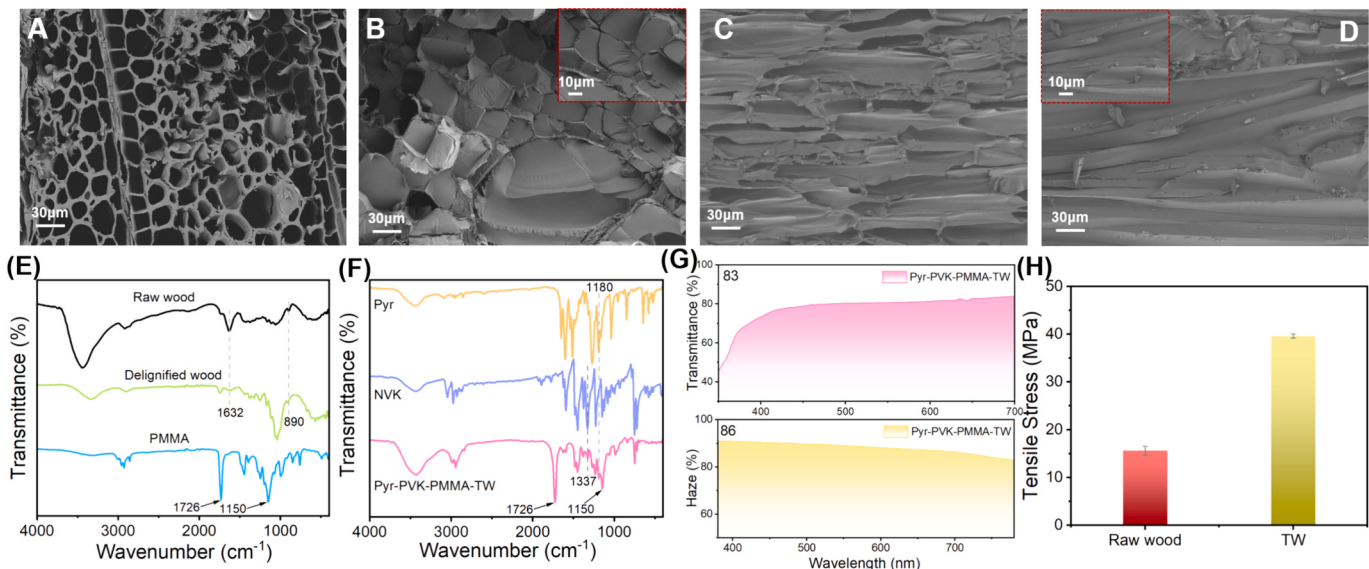


**Fig. 3.** Longitudinal-sectional SEM images of (A) raw wood and (B) Pyr-PVK-PMMA-TW. Cross-sectional SEM images of (C) raw wood and (D) Pyr-PVK-PMMA-TW. (E) FT-IR of raw wood, delignified wood and PMMA. (F) FT-IR of Pyr, NVK and Pyr-PVK-PMMA-TW. (G) Transmittance and haze of Pyr-PVK-PMMA-TW systems. (H) Tensile stress of raw wood and Pyr-PVK-PMMA-TW.

C–N bond stretching vibration between nitrogen atom and adjacent carbon atom in carbazole ring at  $1337\text{ cm}^{-1}$  also indicates the successful preparation of four-component OLPL transparent wood (Fig. 3F) [68,81]. Pyr-PVK-PMMA-TW materials exhibited a transmittance of 83 %, with haze values surpassing 86 % (Fig. 3G). The remarkable transmittance of TW ensured efficient light collection, while its elevated haze value significantly broadened the illuminated area under identical lighting conditions. In contrast to glass materials, which lack significant light scattering capabilities, TW offered greater versatility in the utilization of light [9]. This attribute holds immense significance in the construction of indoor lighting structures, facilitating the achievement of uniform illumination [2]. Furthermore, in terms of tensile stress, transparent wood is more than three times that of raw wood (Fig. 3H) and it also has good hydrophobicity (Fig. S9), so it has bright future in practical application fields.

### 3.3. Pyr-PVK-PMMA photophysical properties

To explore the mechanism of organic long afterglow, we prepare a three-component organic afterglow material formed by Pyr, NVK, and PMMA. It was found that the organic afterglow of the three components, like the four components, also exhibits OLPL afterglow phenomenon (Fig. 4A). The steady-state emission spectrum of Pyr-PVK-PMMA materials is at 596 nm, and the delayed emission (delayed 1 ms) spectrum is also at 596 nm (Fig. 4B, C). The delayed emission intensity at room temperature (excited at 433 nm) follows power-law decay (Fig. 4D, E), which is proportional to  $t^{-m}$ , where the index  $m$  can be marked 1.03. For

OLPL systems, the  $m$  value is usually in the range from 0 to 2, which can describe the rate of charge recombination according to Debye–Edwards law [63]. For the Pyr-PVK-PMMA materials, transient absorption spectra (by 355 nm pump laser) show the positive signals of pyrylium radical in the range of 500–900 nm and the positive signals of PVK radical cation ranging from 1000 nm to 1400 nm (Fig. S10). The negative signals in 400–500 nm of the transient absorption spectra are attributed to PVK fluorescence. The power-law decay behavior and the transient absorption spectra suggest that the OLPL originates from the retarded charge recombination of pyrylium radical and PVK radical cation, while the radical intermediates are formed by photo-induced charge separation. Unlike most reported n-type OLPL systems that are easily quenched by oxygen in the air, the present systems feature p-type mechanism which would be relatively stable under ambient conditions [62,67].

### 3.4. Pyr-PMMA photophysical properties

To further investigate the OLPL mechanism, we split the three-component Pyr-PVK-PMMA system into two-component Pyr-PMMA and Pyr-PVK samples. When Pyr was dissolved in methyl methacrylate (MMA) at 0.01 wt%, a two-component system Pyr-PMMA with a solid transparent glass state was obtained by UV curing for 10 min. Blue-green emission was observed under excitation at 365 and 420 nm lamp and after the excitation was stopped (Fig. 5A). The room-temperature steady-state emission spectrum of Pyr-PMMA is consistent with the delayed emission spectrum (1 ms delay), both of which exhibit a band from 420 to 600 nm with emission maxima at 484 nm (Fig. 5C–E). For

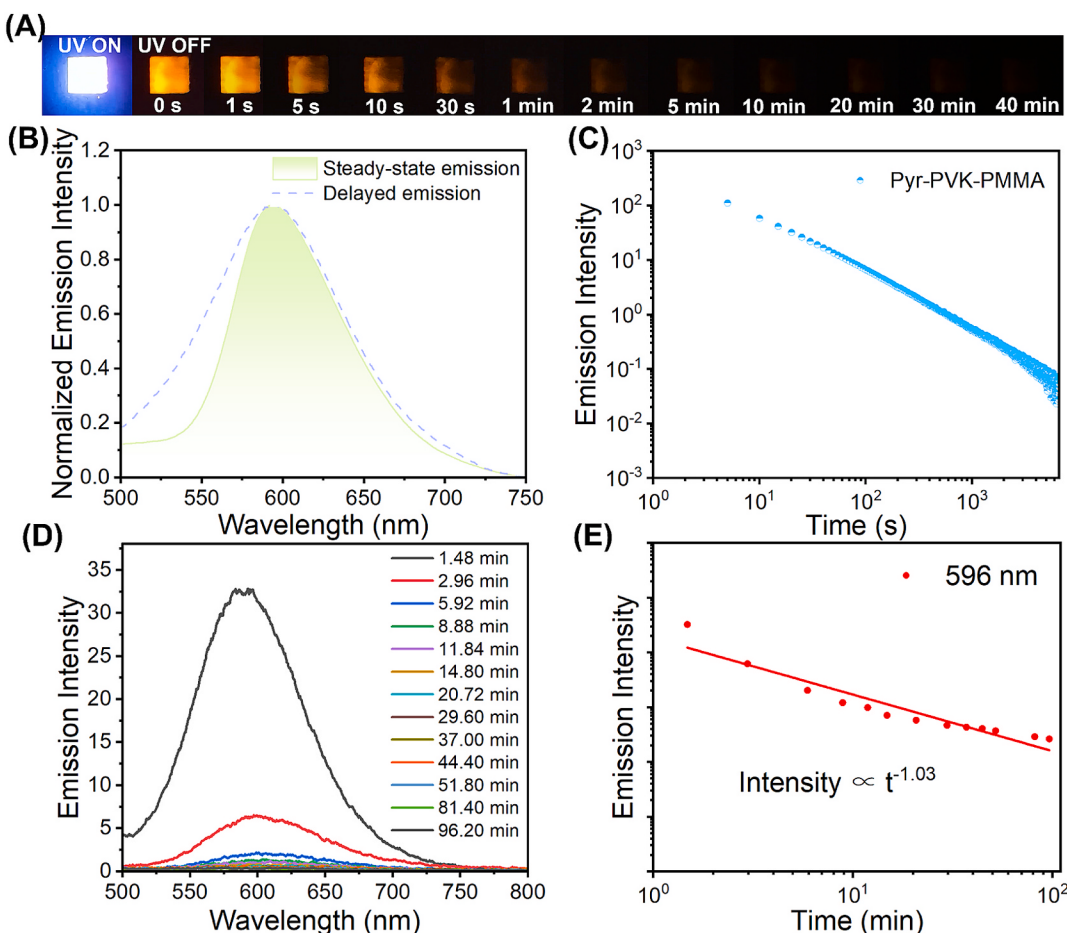


**Fig. 4.** (A) Photographs of 0.1 %Pyr-PVK-PMMA materials under UV lamp and after removal of the excitation sources. (B) Room-temperature steady-state emission and delayed emission (1 ms delay) spectra of 0.1 %Pyr-PVK-PMMA materials excited at 433 nm. (C) Room-temperature emission decay of 0.1 %Pyr-PVK-PMMA materials monitored at 596 nm. (D) OLPL spectra of the 0.1 %Pyr-PVK-PMMA materials as a function of delay times excited at 433 nm. (E) A logarithmic plot of the OLPL decay profile of 0.1 %Pyr-PVK-PMMA materials monitored at a peak wavelength of 596 nm.

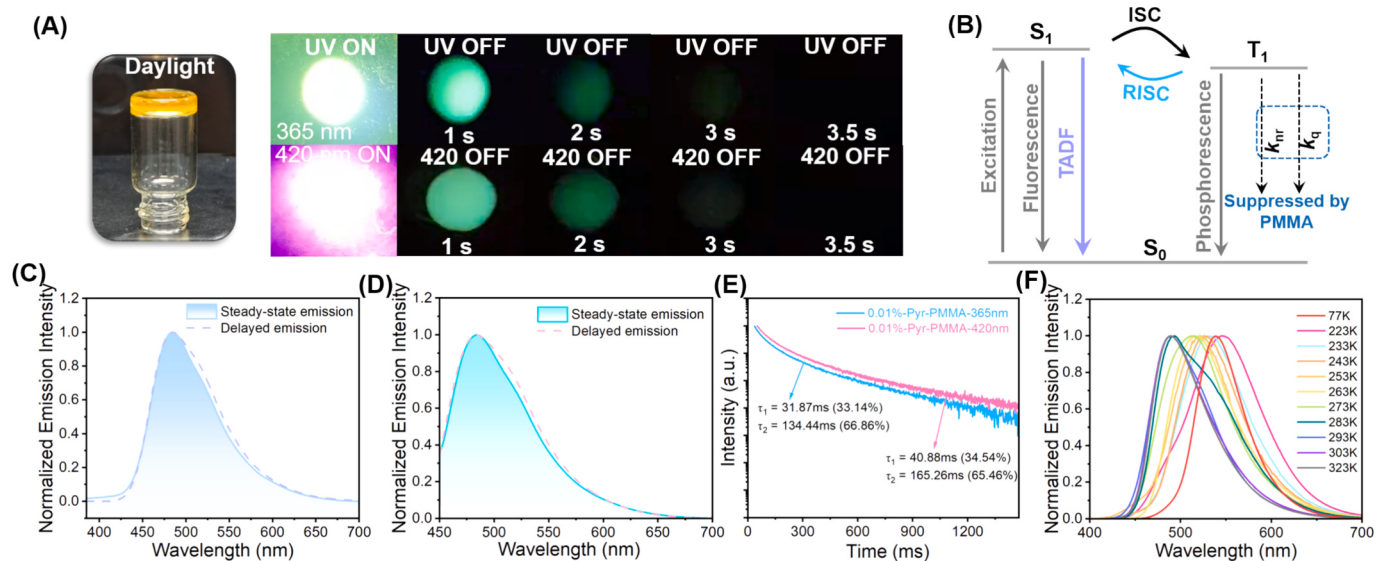


**Fig. 5.** (A) Photographs of 0.01 %Pyr-PMMA materials under 365 nm UV lamp and 420 nm lasers and after removal of the excitation sources. (B) The proposed TADF-type afterglow mechanism in the Pyr-PMMA system which features moderate  $k_{RISC}$  of  $10^0\text{--}10^1\text{ s}^{-1}$ . (C) Room-temperature steady-state emission and delayed emission (1 ms delay) spectra of 0.01 %Pyr-PMMA materials excited at 365 nm. (D) Room-temperature steady-state emission and delayed emission (1 ms delay) spectra of 0.01 %Pyr-PMMA materials excited at 420 nm. (E) Room-temperature excited state decay profile and its fitting of 0.01 %Pyr-PMMA material excited at 365 nm and 420 nm and both monitored at 484 nm. (F) Variable temperature delayed emission spectra (1 ms delay) of 0.01 %Pyr-PMMA materials.

mechanism study, high purity of pyrylium salt can rule out the impurity mechanism (Fig. S7A) [82]. Additionally, reports have suggested that excited state energy transfer from RTP donors to luminescent acceptors can lead to organic afterglow at room temperature [69,70,83,84]. Here the afterglow emission of Pyr-PMMA samples could be excited by 365 nm UV, but due to PMMA's negligible UV-vis absorption at 365 nm (Fig. 5A, C, E), the possibility of excited state energy transfer from PMMA to Pyr is ruled out. Thirdly, since PMMA possessing low-lying HOMO ( $-7.53\text{ eV}$ ) and high-lying LUMO ( $-0.05\text{ eV}$ ) when compared to Pyr dopants (HOMO:  $-6.35\text{ eV}$ , LUMO:  $-3.95\text{ eV}$ ), intermolecular charge transfer between Pyr and PMMA would be insignificant and thus the organic long persistent luminescence mechanism can be ruled out in PMMA system [55]. Furthermore, the mediation of singlet-to-triplet intersystem crossing (ISC) by triplet excited states of organic matrices, leading to the emergence of room-temperature afterglow [85], was not the case in the Pyr-PMMA system. This is due to the higher  $T_1$  level of PMMA compared to Pyr's  $S_1$  and  $T_1$  states.

To investigate the afterglow mechanism of Pyr-PMMA, temperature-dependent delayed emission studies have been performed to show that a delayed emission band at 539 nm (2.30 eV) is observed at 77 K (Fig. 5F). The delayed emission band at 484 nm increases with temperature and is more favorable at room temperature and above. Due to its emission maximum being the same as or very close to the steady-state emission spectrum, the 484 nm delayed emission band can be assigned to the delayed fluorescence of Pyr-PMMA sample with an  $S_1$  energy level of 2.55 eV, which supports the thermally activated delayed fluorescence (TADF) mechanism (Fig. 5B); at low doing concentration of 0.01 %, delayed fluorescence caused by triplet-triplet annihilation would be insignificant. With reference to our previous study on TADF-type organic afterglow [58], here the moderate singlet-triplet splitting energy ( $\Delta E_{ST}$ , 0.25 eV) in Pyr-PMMA system and ISC/RISC channels with spin-orbit coupling matrix elements of around  $0.3\text{ cm}^{-1}$  (Fig. S11) would be suitable to open a RISC pathway with moderate rate constant  $k_{RISC}$  of  $10^0\text{--}10^1\text{ s}^{-1}$  to harvest triplet excitons and maintain long emission lifetimes at room temperature (Fig. 5B). PMMA matrix protect organic triplet excitons by its rigid microenvironment.

### 3.5. Pyr-PVK photophysical properties

We also tested the photocatalytic properties of Pyr using the monomer NVK. A red-orange Pyr-PVK system lasting for one hour was obtained by photopolymerization, with a maximum emission wavelength of 607 nm under 433 nm excitation at room temperature (Fig. 6A). The afterglow intensity obeys the power law decay and is proportional to  $t^{-m}$ , where the index  $m$  can be marked 1.05. The duration of more than 1 h and the power law decay indicate that there is an OLPL mechanism in the Pyr-PVK system caused by the delay of charge recombination in the glassy PVK matrix (Fig. 6B-D). PVK polymer, NVK solid and Pyr-NVK materials do not show long afterglow at room temperature (Fig. S12). After UV irradiation, PVK (HOMO,  $-5.29\text{ eV}$ ; LUMO,  $-1.80\text{ eV}$ ) and Pyr (HOMO,  $-6.53\text{ eV}$ ; LUMO,  $-3.95\text{ eV}$ ) form a complex with emission maxima at 607 nm (2.04 eV) in the steady-state emission spectrum, which is longer than the steady-state spectra of Pyr-PMMA samples and Pyr solutions in dichloromethane. These observations are consistent with the photophysical phenomenon of the reported OLPL system [63,68].

The OLPL system assumes intermolecular charge transfer characteristics with almost degenerate of  $S_1$  and  $T_1$  energy levels. Such  $S_1$  and  $T_1$  levels are lower than the  $T_1$  level of Pyr (2.30 eV), which blocks the energy transfer path from the Pyr-PVK to the  $T_1$  state of Pyr (Fig. 6E). Therefore, photo-induced charge separation occurs in the Pyr-PVK system, forming Pyr free radicals and PVK radical cations. Subsequently, the retarded charge recombination gives rise to OLPL phenomenon (Fig. 6E).

### 3.6. Properties of OLPL wood coating, adhesive and wood-plastic composite

In addition to transparent wood, to expand the development of wood-based products, we applied Pyr-PVK-PMMA to coat on wood (Fig. 7A), and under UV light excitation, we obtained an OLPL wood coating (Fig. 7B, S15). The surface of the coating is smooth and even (Fig. 7D) with excellent hydrophobic properties, and the water contact angle decreased only slightly from  $113.9^\circ$  to  $113.5^\circ$  at 30 s (Fig. 7C). Compared to the reported literatures where the materials have tensile stress of 25–45 MPa, the wood coated with a 1 mm layer of the OLPL

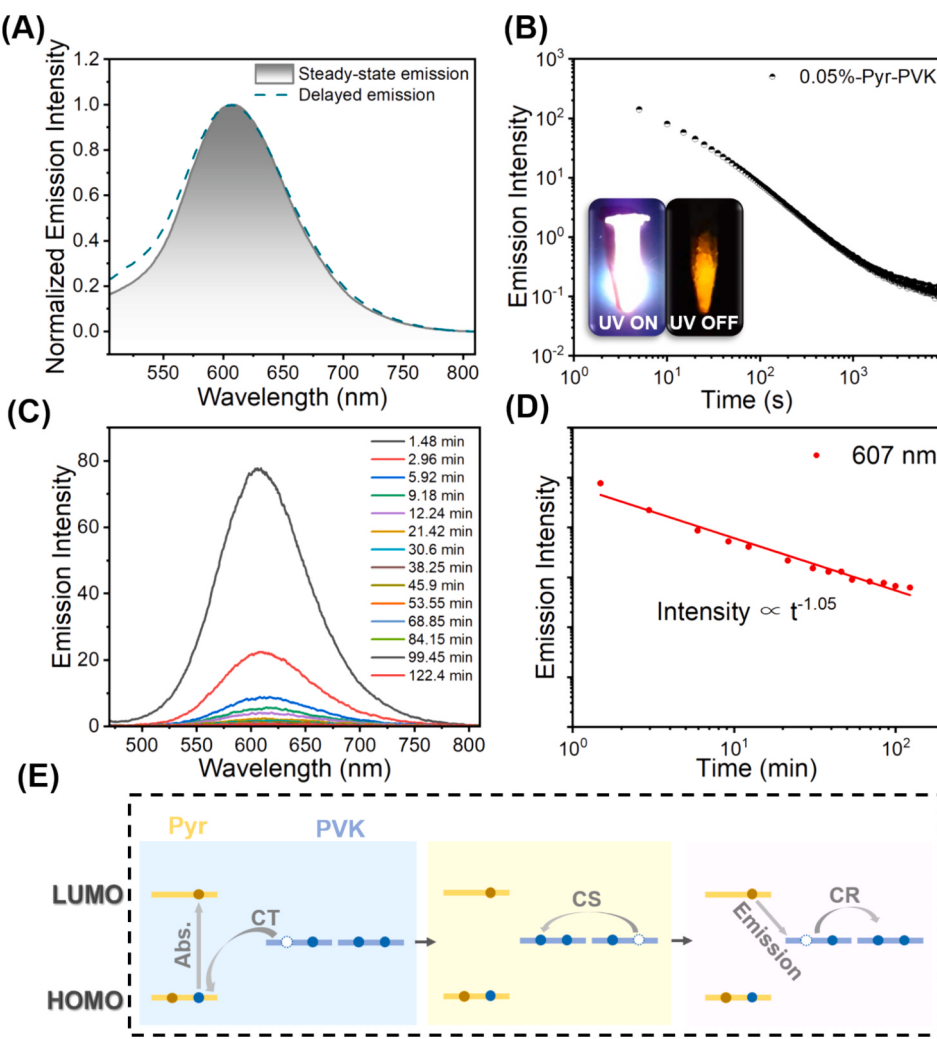


**Fig. 6.** (A) Room-temperature steady-state emission and delayed emission (1 ms delay) spectra of 0.05 %Pyr-PVK materials excited at 433 nm. (B) Room-temperature emission decay of 0.05 %Pyr-PVK materials excited at 433 nm and monitored at 607 nm. (C) OLPL spectra of the 0.05 %Pyr-PVK materials as a function of delay times (excited at 433 nm). (D) A logarithmic plot of the OLPL decay profile of 0.05 %Pyr-PVK materials monitored at a peak wavelength of 607 nm. (E) Proposed emission mechanism of the Pyr-PVK OLPL system with relevant HOMO–LUMO energy level diagrams of materials.

coating exhibits a higher tensile stress of 49.82 MPa (Fig. 7E) [86,87]. Additionally, when ink was dropped onto the coating wood and subsequently wiped off, no stains remained (Fig. 7F). Afterglow devices may be susceptible to contamination during usage, which can affect their aesthetics and clarity, so anti-sewage or anti-fouling property is important for the long-term service of afterglow devices. When contaminated water was dripped onto the surface at a 45° tilt, it slid off smoothly (Fig. 7G). These indicates that the Pyr-PVK-PMMA system, as a wood coating, demonstrates superior performance in enhancing mechanical properties, water resistance, and anti-fouling capabilities. Furthermore, we used Pyr-PVK-UV curable resin glue (with PMMA as the primary component) to bond wood boards (Fig. 7H, 7I, S14), resulting in an OLPL wood adhesive with a tensile strength of 22.37 MPa, significantly better than bio-based adhesives (Fig. 7J) [88,89]. Phenolic resin, urea formaldehyde resin and other traditional wood adhesives may have better mechanical property than the present OLPL wood adhesives, but some of these traditional adhesives could release formaldehyde, which would be harmful to human health and the environment.

Subsequently, we prepared an OLPL wood-plastic composite containing 10 % wood powder (Fig. 8B, S15). This composite not only exhibits excellent long afterglow performance but also possesses good processability (Fig. 8A). SEM observations reveal the dispersion of wood

powder within the Pyr-PVK-PMMA matrix and the interfacial adhesion between the reinforcing materials. It is evident that the wood powder is well integrated into the Pyr-PVK-PMMA system without any phase separation or voids, indicating a strong interaction between the wood flour and the matrix (Fig. 8C). Tensile test results further confirm that this OLPL wood-plastic composite possesses significant mechanical strength (Fig. 8D) [90–94] and the water contact angle of 90.6° also indicates its excellent water resistance (Fig. 8E).

### 3.7. Material functions

OLPL wood-based materials stand out as eco-friendly construction materials with unique photoluminescence properties. They not only inherit the natural biodegradability and low environmental impact of wood but also achieve sustained luminescence without external light sources, providing new dimensions for architectural design. Additionally, the application of these materials helps reduce reliance on traditional electric light sources, thereby lowering energy consumption and aligning with the principles of sustainable development. Whether in the construction industry or other application scenarios, OLPL wood materials have many applications, which can be prepared into luminescent materials of different shapes. For example, we cut transparent wood to obtain an afterglow grass (Fig. 9A), which gives OLPL afterglow wood

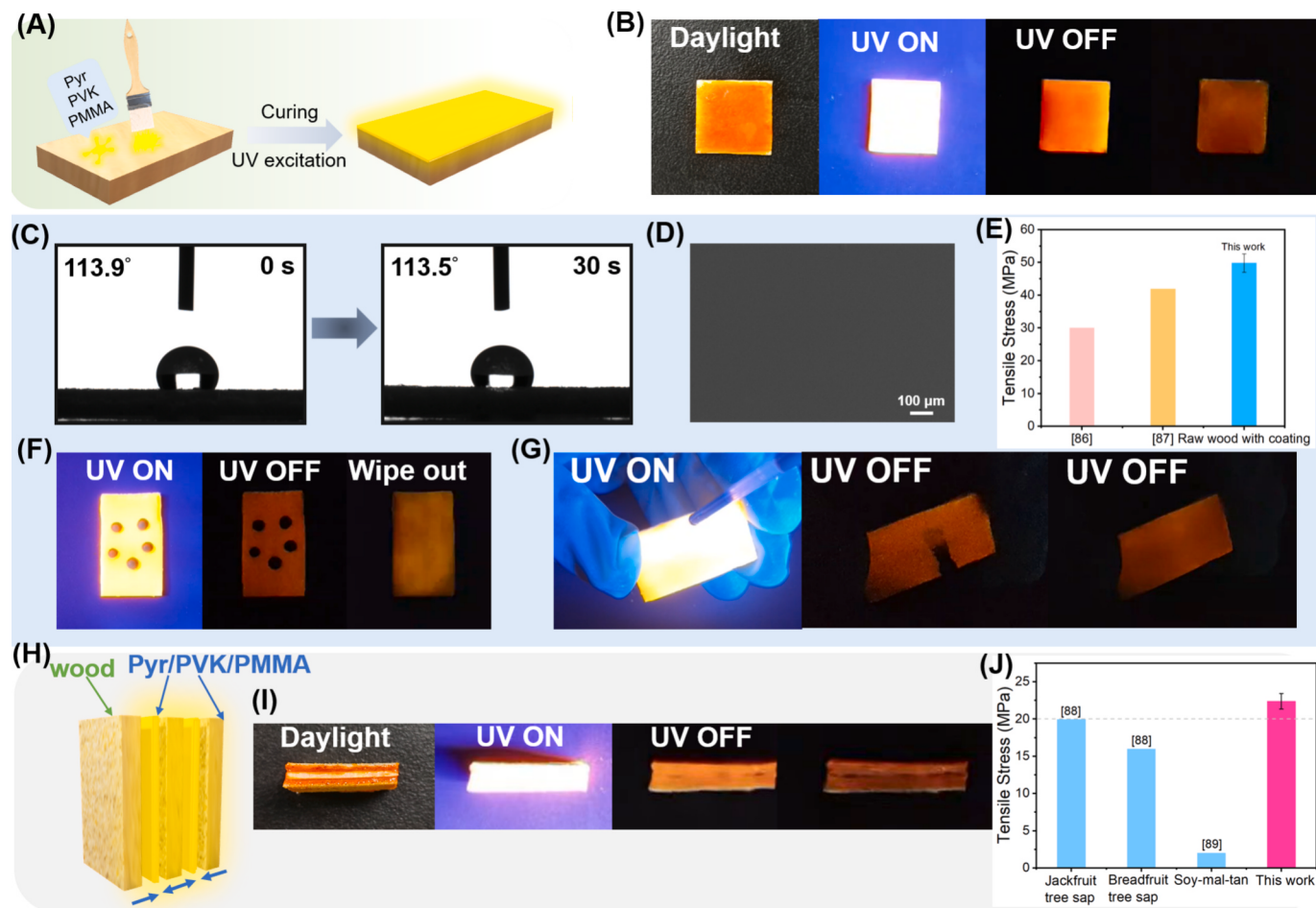


**Fig. 7.** (A) Schematic diagram for the preparation of OLPL wood coatings. (B) Photographs of OLPL wood coatings under UV lamp and after removal of the excitation sources. (C) Water contact angle of OLPL wood coatings. (D) SEM images of OLPL wood coatings. (E) Tensile stress of OLPL wood coatings. (F) Photographs of OLPL wood coatings exhibiting the capability of repelling sewage (water droplets with black ink was used to mimic sewage). (H) Schematic diagram of OLPL wood adhesive preparation. (I) Photographs of OLPL wood adhesive under UV lamp and after removal of the excitation sources. (J) Tensile stress of OLPL wood adhesive.

excellent processability. We combined the afterglow transparent wood panels with the safety exit pattern for emergency lighting (Fig. 9B). Applying the OLPL coating onto wooden carvings of rabbit can also make them emit light (Fig. 9D) to prepare high-quality handicrafts. In the application of wooden puzzles, we apply the OLPL wood coating to the middle piece, which is clearly reflected when the UV light is turned on and off (Fig. 9C). This is of great significance for anti-counterfeiting in advanced puzzles. In addition, we prepared OLPL wood-plastic materials in the shape of wooden piles using silicone resin molds (Fig. 9E, F), which demonstrates the universality of luminescent systems. Finally, we can freely print various patterns on OLPL transparent wood panels, making it possible to tailor products to individual needs (Fig. 9G, H). In short, transparent wood with long afterglow has shown broad application prospects in multiple fields due to its unique advantages.

#### 4. Conclusion

In conclusion, we have prepared an unprecedented OLPL transparent wood material with emission maxima at approximately 596 nm and lasting for more than 1 h. The combination of wood and PMMA as a matrix can provide a rigid environment for Pyr systems and act as an oxygen barrier, inhibiting non-radiative decay and oxygen quenching. The collaboration of wood and synthetic polymers not only increase mechanical property but also provides better microenvironment to protect organic long-lived excitons and radical intermediates. To

investigate the OLPL mechanism, we separated the four-component system. In the Pyr-PMMA system, the materials exhibit TADF-type afterglow behaviors, while the two-component of Pyr-PVK displays an organic long persistent luminescence phenomenon. Specially, it blocks the population of Pyr's  $T_1$  states because of the lower energy levels of the exciplex and opens the charge separation plus retarded charge recombination pathway, giving rise to hour-long OLPL properties of the hole diffusion mechanism against the influence of oxygen under ambient conditions. Moreover, we have also prepared other OLPL wood-based materials, including coatings, adhesives, and wood-plastic composites.

We estimate the cost of OLPL transparent wood to be ¥32534/ton (\$4463/ton) in Table S2. Such cost is much higher than traditional building materials such as glass (¥1000 ~ 2000/ton) and stone (¥1000 ~ 3000/ton), higher than PMMA (¥18000 ~ 20000/ton), but much lower than most of other sustainable afterglow materials [95]. In view of the superior afterglow property and diverse functions, the OLPL transparent wood has high cost-effectiveness. With reference to the reported study [96], the industrial fabrication of transparent wood (1 kg of forest biomass is considered as raw material) leads to environmental impact values of 169 kg CO<sub>2</sub> equivalent. For the end-of-life analysis of transparent wood, the wood can be degraded by incineration and landfilling, while the synthetic polymers can be degraded by incineration. The environmental impacts generated during end-of-life of transparent wood have lower values than conventional plastics such as polyethylene. We use these results to describe the environment impacts of the OLPL

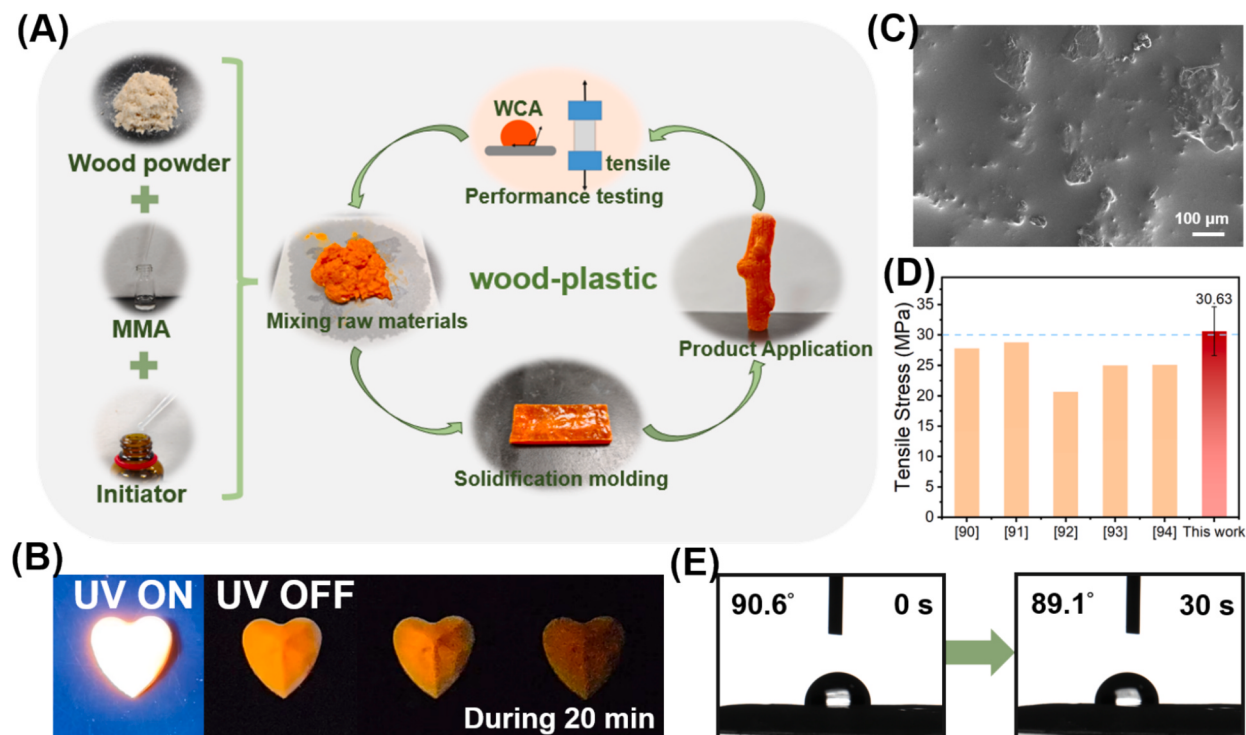


**Fig. 8.** (A) Schematic diagram for the preparation of OLPL wood-plastic composite. (B) Photographs of OLPL heart shaped wood-plastic composite under UV lamp and after removal of the excitation sources. (C) SEM images of OLPL wood-plastic composite. (D) Comparison between the tensile stress of OLPL wood-plastic composite and other literature. (E) Water contact angle of OLPL wood-plastic composite.

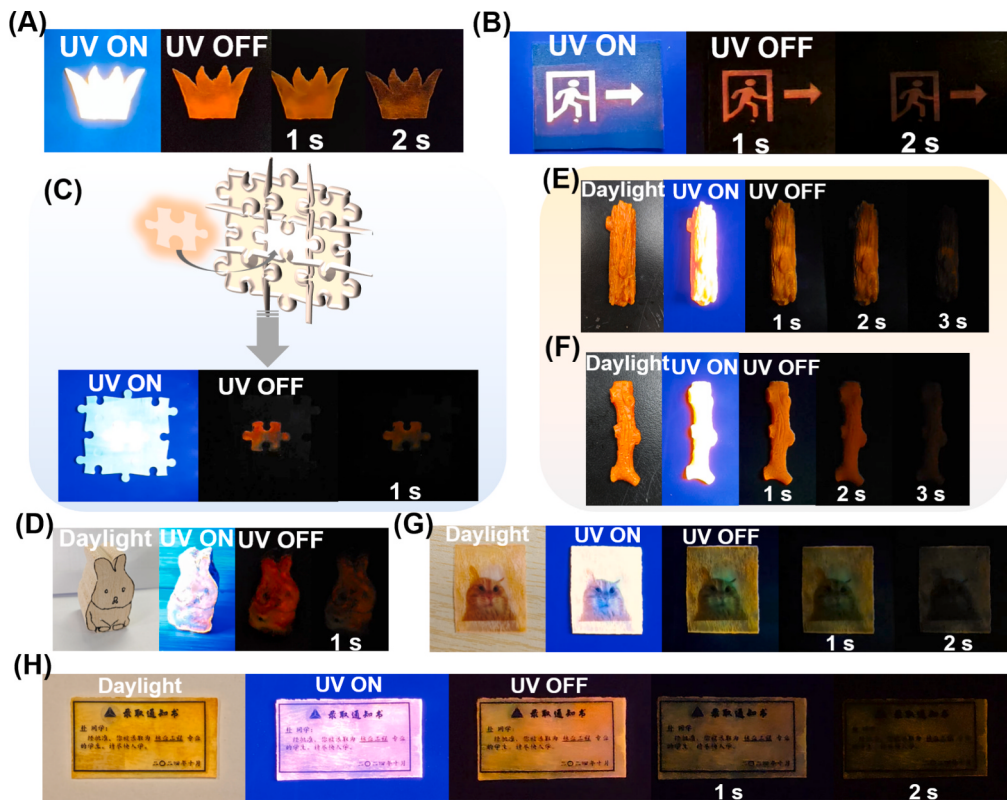


**Fig. 9.** (A) OLPL wood cut into small grass patterns. (B) Safety exit made from OLPL wood panel for emergency lighting. (C) The central piece is a luminous wooden puzzle. (D) Luminous wood carving in the shape of a little rabbit. (E) Luminous wood plastic composite material with large wooden pile pattern. (F) Luminous wood plastic composite material with small wooden stake pattern. (G) 3D printing of kitten patterns and (H) admission letter patterns on luminescent transparent wood.

transparent wood in the present study, since the compositions of the OLPL transparent wood is not significantly different from transparent wood in the reported study [96]. Therefore, wood-based materials with long-lasting afterglow will have a very broad application prospect in the future.

### CRediT authorship contribution statement

**Xixi Piao:** Writing – original draft, Methodology, Data curation. **Zhengwen Ning:** Visualization, Data curation. **Qingxin He:** Visualization, Data curation. **Yue Zhang:** Visualization, Data curation. **Tengyue Wang:** Visualization. **Guangming Wang:** Visualization. **Kaka Zhang:** Writing – review & editing, Supervision, Funding acquisition, Conceptualization.

### Declaration of competing interest

The authors declare that they have no known competing financial interests or personal relationships that could have appeared to influence the work reported in this paper.

### Acknowledgements

We thank the financial supports from National Natural Science Foundation of China (22475228, 22175194), the Strategic Priority Research Program of the Chinese Academy of Sciences (XDB0610000), Hundred Talents Program from Shanghai Institute of Organic Chemistry (Y121078), Pioneer Hundred Talents Program of Chinese Academy of Sciences (E320021), and Ningbo Natural Science Foundation (2023J243).

### Appendix A. Supplementary data

Supplementary data to this article can be found online at <https://doi.org/10.1016/j.cej.2025.160718>.

### Data availability

Data will be made available on request.

### References

- [1] Y. Hu, F. Hu, M. Gan, Y. Xie, Q. Feng, Facile one-step fabrication of all cellulose composites with unique optical performance from wood and bamboo pulp, *Carbohydr. Polym.* 274 (2021) 118630, <https://doi.org/10.1016/j.carbpol.2021.118630>.
- [2] X. Wang, T. Zhan, Y. Liu, J. Shi, B. Pan, Y. Zhang, L. Cai, S.Q. Shi, Large-size transparent wood for energy-saving building applications, *ChemSusChem* 11 (2018) 4086–4093, <https://doi.org/10.1002/cssc.201801826>.
- [3] Y. Li, Q. Fu, X. Yang, L.A. Berglund, Transparent wood for functional and structural applications, *Philos. Trans. A: Math. Phys. Eng. Sci.* 376 (2018) 2017082, <https://doi.org/10.1098/rsta.2017.0182>.
- [4] Z. Yu, N. Yang, L. Zhou, Z. Ma, Y. Zhu, Y. Lu, B. Qin, W. Xing, T. Ma, S. Li, H. Gao, H. Wu, S. Yu, Bioinspired polymeric woods, *Sci. Adv.* 4 (2018) 7223, <https://doi.org/10.1126/sciadv.aat7223>.
- [5] F. Jiang, T. Li, Y. Li, Y. Zhang, A. Gong, J. Dai, E. Hitz, W. Luo, L. Hu, Wood-based nanotechnologies toward sustainability, *Adv. Mater.* 30 (2018) 1703453, <https://doi.org/10.1002/adma.201703453>.
- [6] C. Montanari, Y. Li, H. Chen, M. Yan, L.A. Berglund, Transparent wood for thermal energy storage and reversible optical transmittance, *ACS Appl. Mater. Interfaces* 11 (2019) 20465–20472, <https://doi.org/10.1021/acsami.9b05525>.
- [7] T. Li, Y. Zhai, S. He, W. Gan, Z. Wei, M. Heidarinejad, D. Dalgo, R. Mi, X. Zhao, J. Song, J. Dai, C. Chen, A. Aili, A. Vellore, A. Martini, R. Yang, J. Srebric, X. Yin, L. Hu, A radiative cooling structural material, *Science* 364 (2019) 760–763, <https://doi.org/10.1126/science.aau9101>.
- [8] Q. Fu, Y. Chen, M. Sorieul, Wood-based flexible electronics, *ACS Nano* 14 (2020) 3528–3538, <https://doi.org/10.1021/acsnano.9b09817>.
- [9] Q. Xia, C. Chen, T. Li, S. He, J. Gao, X. Wang, L. Hu, Solar-assisted fabrication of large-scale, patternable transparent wood, *Sci. Adv.* 7 (2021) eabd7342, <https://doi.org/10.1126/sciadv.abd7342>.
- [10] Y. Zhang, H. Xiao, R. Xiong, C. Huang, Xylan-based ratiometric fluorescence carbon dots composite with delignified wood for highly efficient water purification and photothermal conversion, *Sep. Purif. Technol.* 324 (2023) 124513, <https://doi.org/10.1016/j.seppur.2023.124513>.
- [11] C. Cai, Y. Sun, Y. Chen, Z. Wei, Y. Wang, F. Chen, W. Cai, J. Ji, Y. Ji, Y. Fu, Large scalable, ultrathin and self-cleaning cellulose aerogel film for daytime radiative cooling, *J. Bioresour. Bioprod.* 8 (2023) 421–429, <https://doi.org/10.1016/j.jbab.2023.06.004>.
- [12] Y.I. Golovin, A.A. Gusev, D.Y. Golovin, S.M. Matveev, A.I. Tyrin, A.A. Samodurov, V.V. Korenkov, I.A. Vasukova, M.A. Yunack, Multiscale wood micromechanics and size effects study via nanoindentation, *J. Bioresour. Bioprod.* 8 (2023) 246–264, <https://doi.org/10.1016/j.jobab.2023.04.002>.
- [13] Z. Lü, Q. Gao, M. Shi, Z. Su, G. Chen, H. Qi, B. Li, F. Peng, Colorful room-temperature phosphorescence including white afterglow from mechanical robust transparent wood for time delay lighting, *Small Struct.* 5 (2024) 2300567, <https://doi.org/10.1002/sstr.202300567>.
- [14] S. Wang, L. Li, L. Zha, S. Koskela, L.A. Berglund, Q. Zhou, Wood xerogel for fabrication of high-performance transparent wood, *Nat. Commun.* 14 (2023) 2827, <https://doi.org/10.1038/s41467-023-38481-x>.
- [15] M. Zhu, J. Song, T. Li, A. Gong, Y. Wang, J. Dai, Y. Yao, W. Luo, D. Henderson, L. Hu, Highly anisotropic, highly transparent wood composites, *Adv. Mater.* 28 (2016) 5181–5187, <https://doi.org/10.1002/adma.201600427>.
- [16] R. Mi, C. Chen, T. Keplinger, Y. Pei, S. He, D. Liu, J. Li, J. Dai, E. Hitz, B. Yang, I. Burgert, L. Hu, Scalable aesthetic transparent wood for energy efficient buildings, *Nat. Commun.* 11 (2020) 3836, <https://doi.org/10.1038/s41467-020-17513-w>.
- [17] Q. Fu, K. Tu, C. Goldhahn, T. Keplinger, M. Adobes-Vidal, M. Sorieul, I. Burgert, Luminescent and hydrophobic wood films as optical lighting materials, *ACS Nano* 14 (2020) 13775–13783, <https://doi.org/10.1021/acsnano.0c06110>.
- [18] Z. Bi, T. Li, H. Su, Y. Ni, L. Yan, Transparent wood film incorporating carbon dots as encapsulating material for white light-emitting diodes, *ACS Sustain. Chem. Eng.* 6 (2018) 9314–9323, <https://doi.org/10.1021/acssuschemeng.8b01618>.
- [19] Q. Fu, M. Yan, E. Jungstedt, X. Yang, Y. Li, L.A. Berglund, Transparent plywood as a load-bearing and luminescent biocomposite, *Compos. Sci. Technol.* 164 (2018) 296–303, <https://doi.org/10.1016/j.compscitech.2018.06.001>.
- [20] J. Yuan, Y. Zhai, K. Wan, S. Liu, J. Li, S. Li, Z. Chen, T.D. James, Sustainable afterglow materials from lignin inspired by wood phosphorescence, *Cell Rep. Phys. Sci.* 2 (2021) 100542, <https://doi.org/10.1016/j.xrpp.2021.100542>.
- [21] H. Yuan, T. Ren, Q. Luo, Y. Huang, Y. Huang, D. Xu, X. Guo, X. Li, Y. Wu, Fluorescent wood with non-cytotoxicity for effective adsorption and sensitive detection of heavy metals, *J. Hazard. Mater.* 416 (2021) 126166, <https://doi.org/10.1016/j.jhazmat.2021.126166>.
- [22] K. Wan, B. Tian, Y. Zhai, Y. Liu, H. Wang, S. Liu, S. Li, W. Ye, Z. An, C. Li, J. Li, T. D. James, Z. Chen, Structural materials with afterglow room temperature phosphorescence activated by lignin oxidation, *Nat. Commun.* 13 (2022) 5508, <https://doi.org/10.1038/s41467-022-33273-1>.
- [23] Y. Zhai, S. Li, J. Li, S. Liu, T.D. James, J.L. Sessler, Z. Chen, Room temperature phosphorescence from natural wood activated by external chloride anion treatment, *Nat. Commun.* 14 (2023) 2614, <https://doi.org/10.1038/s41467-023-37762-9>.
- [24] Y. Liu, H. Yang, C. Ma, S. Luo, M. Xu, Z. Wu, W. Li, S. Liu, Luminescent transparent wood based on lignin-derived carbon dots as a building material for dual-channel, real-time, and visual detection of formaldehyde gas, *ACS Appl. Mater. Interfaces* 12 (2020) 36628–36638, <https://doi.org/10.1021/acsmami.0c10240>.
- [25] R. Liu, H. Guo, M. Cao, B. Dang, Y. Zhai, S. Liu, S. Li, J. Li, T.D. James, Z. Chen, Producing a room temperature phosphorescent film from natural wood using a top-down approach, *Adv. Funct. Mater.* 34 (2023) 2312254, <https://doi.org/10.1002/adfm.202312254>.
- [26] T. Cheng, H. Zhang, K. Cao, Y. Jing, Y. Wu, First development of transparent wood-based triboelectric nanogenerator (TW-TENG): Cooperative incorporation of transparency, aesthetic of wood, and superior triboelectric properties, *Nano Energy* 128 (2024) 109888, <https://doi.org/10.1016/j.nanoen.2024.109888>.
- [27] Y. Chen, B. Dang, C. Wang, Y. Wang, Y. Yang, M. Liu, H. Bi, D. Sun, Y. Li, J. Li, X. Shen, Q. Sun, Intelligent designs from nature: Biomimetic applications in wood technology, *Prog. Mater. Sci.* 139 (2023) 101164, <https://doi.org/10.1016/j.pmatsci.2023.101164>.
- [28] L. Zhang, S. Lyu, Z. Chen, S. Wang, Preparation and characterization of dual-functional coatings of nanofibrillated cellulose and modified SrAl<sub>2</sub>O<sub>4</sub>: Eu, Dy phosphors, *Surf. Coat. Tech.* 349 (2018) 318–327, <https://doi.org/10.1016/j.surfcoat.2018.05.071>.
- [29] Q. Li, J. Qin, S. Li, X. Zhao, Y. Hu, Transparent fiber wood composite materials containing long afterglow as lighting equipment, *J. Appl. Polym. Sci.* 137 (2020) 49203, <https://doi.org/10.1002/app.49203>.
- [30] G. Xiong, Z. Zhang, Y. Qi, Effect of the properties of long afterglow phosphors on the antifouling performance of silicone fouling-release coating, *Prog. Org. Coat.* 170 (2022) 106965, <https://doi.org/10.1016/j.porgcoat.2022.106965>.
- [31] J. Luo, B. Ren, X. Zhang, M. Zhu, T. Liang, Z. Huang, Y. Zheng, X. Li, J. Li, Z. Zheng, B. Chen, Y. Fu, D. Tu, Y. Wang, Y. Jia, D. Peng, Modulating smart mechanoluminescent phosphors for multistimuli responsive optical wood, *Adv. Sci.* 11 (2024) 2305066, <https://doi.org/10.1002/advs.202305066>.
- [32] J. Zhou, B. Tian, Y. Zhai, M. Wang, S. Liu, J. Li, S. Li, T.D. James, Z. Chen, Photoactivated room temperature phosphorescence from lignin, *Nat. Commun.* 15 (2024) 7198, <https://doi.org/10.1038/s41467-024-51545-w>.
- [33] V.-W.-W. Yam, V.-K.-M. Au, S.-Y.-L. Leung, Light-emitting self-assembled materials based on d<sup>8</sup> and d<sup>10</sup> transition metal complexes, *Chem. Rev.* 115 (2015) 7589–7728, <https://doi.org/10.1021/cr.acschemrev.5b00074>.
- [34] K. Zhang, Q. Yu, H. Wei, S. Liu, Q. Zhao, W. Huang, Long-lived emissive probes for time-resolved photoluminescence bioimaging and biosensing, *Chem. Rev.* 118 (2018) 1770–1839, <https://doi.org/10.1021/acs.chemrev.7b00425>.

- [35] H. Uoyama, K. Goushi, K. Shizu, H. Nomura, C. Adachi, Highly efficient organic light-emitting diodes from delayed fluorescence, *Nature* 492 (2012) 234–238, <https://doi.org/10.1038/nature11687>.
- [36] Z. Guan, Z. Tang, J. Deng, Y. Zheng, H. Li, X. Liu, Multi-color pure organic room temperature phosphorescent materials with long lifetime and high efficiency, *Adv. Funct. Mater.* 34 (2023) 2310198, <https://doi.org/10.1002/adfm.202310198>.
- [37] X. Ma, J. Wang, H. Tian, Assembling-induced emission: an efficient approach for amorphous metal-free organic emitting materials with room-temperature phosphorescence, *Acc. Chem. Res.* 52 (2019) 738–748, <https://doi.org/10.1021/acs.accounts.8b00620>.
- [38] C. Kenry, B. Chen, Liu, Enhancing the performance of pure organic room-temperature phosphorescent luminophores, *Nat. Commun.* 10 (2019) 2111, <https://doi.org/10.1038/s41467-019-10033-2>.
- [39] W. Zhao, Z. He, B.Z. Tang, Room-temperature phosphorescence from organic aggregates, *Nat. Rev. Mater.* 5 (2020) 869–885, <https://doi.org/10.1038/s41578-020-0223-z>.
- [40] X. Yan, H. Peng, Y. Xiang, J. Wang, L. Yu, Y. Tao, H. Li, W. Huang, R. Chen, Recent advances on host-guest material systems toward organic room temperature phosphorescence, *Small* 18 (2022) 2104073, <https://doi.org/10.1002/smll.202104073>.
- [41] G. Zhang, J. Chen, S.J. Payne, S.E. Kooi, J.N. Demas, C.L. Fraser, Multi-emissive difluoroboron dibenzylmethane polylactide exhibiting intense fluorescence and oxygen-sensitive room-temperature phosphorescence, *J. Am. Chem. Soc.* 129 (2007) 8942–8943, <https://doi.org/10.1021/ja0720255>.
- [42] B. Wu, X. Xu, Y. Tang, X. Han, G. Wang, Multifunctional optical polymeric films with photochromic, fluorescent, and ultra-long room temperature phosphorescent properties, *Adv. Opt. Mater.* 9 (2021) 2101266, <https://doi.org/10.1002/adom.202101266>.
- [43] D. Peng, S. He, Y. Zhang, L. Yao, W. Nie, Z. Liao, W. Cai, X. Ye, Blue light-induced rare-earth free phosphors for the highly sensitive and selective imaging of latent fingerprints based on enhanced hydrophobic interaction, *J. Materomics* 8 (2022) 229–238, <https://doi.org/10.1016/j.jmat.2021.03.005>.
- [44] N. Gan, H. Shi, Z. An, W. Huang, Recent advances in polymer-based metal-free room-temperature phosphorescent materials, *Adv. Funct. Mater.* 28 (2018) 1802657, <https://doi.org/10.1002/adfm.201802657>.
- [45] T. Zhang, X. Ma, H. Wu, L. Zhu, Y. Zhao, H. Tian, Molecular engineering for metal-free amorphous materials with room-temperature phosphorescence, *Angew. Chem. Int. Ed.* 59 (2020) 11206–11216, <https://doi.org/10.1002/anie.201915433>.
- [46] J. Li, G. Wang, X. Chen, X. Li, M. Wu, S. Yuan, Y. Zou, X. Wang, K. Zhang, Manipulation of triplet excited states in two-component systems for high-performance organic afterglow materials, *Chem. -Eur. J.* 28 (2022), <https://doi.org/10.1002/chem.202200852> e202200852.
- [47] S. Guo, W. Dai, X. Chen, Y. Lei, J. Shi, B. Tong, Z. Cai, Y. Dong, Recent progress in pure organic room temperature phosphorescence of small molecular host–guest systems, *ACS Mater. Lett.* 3 (2021) 379–397, <https://doi.org/10.1021/acsmaterialslett.1c00062>.
- [48] H. Gao, X. Ma, Recent progress on pure organic room temperature phosphorescent polymers, *Aggregate* 2 (2021), <https://doi.org/10.1002/agt2.38> e38.
- [49] Q. Li, Z. Li, Molecular packing: another key point for the performance of organic and polymeric optoelectronic materials, *Acc. Chem. Res.* 53 (2020) 962–973, <https://doi.org/10.1021/acs.accounts.0c00060>.
- [50] M. Singh, K. Liu, S. Qu, H. Ma, H. Shi, Z. An, W. Huang, Recent advances of cocrystals with room temperature phosphorescence, *Adv. Opt. Mater.* 9 (2021) 2002197, <https://doi.org/10.1002/adom.202002197>.
- [51] G. Zhang, G.M. Palmer, M.W. Dewhurst, C.L. Fraser, A dual-emissive-materials design concept enables tumour hypoxia imaging, *Nat. Mater.* 8 (2009) 747–751, <https://doi.org/10.1038/NMAT2509>.
- [52] W.Z. Yuan, X.Y. Shen, H. Zhao, J.W.Y. Lam, L. Tang, P. Lu, C. Wang, Y. Liu, Z. Wang, Q. Zheng, J.Z. Sun, Y. Ma, B.Z. Tang, Crystallization-induced phosphorescence of pure organic luminogens at room temperature, *J. Phys. Chem. C* 114 (2010) 6090–6099, <https://doi.org/10.1021/jp909388y>.
- [53] O. Bolton, K. Lee, H.-J. Kim, K.Y. Lin, J. Kim, Activating efficient phosphorescence from purely organic materials by crystal design, *Nat. Chem.* 3 (2011) 205–210, <https://doi.org/10.1038/nchem.984>.
- [54] S. Hirata, K. Totani, J. Zhang, T. Yamashita, H. Kaji, S.R. Marder, T. Watanabe, C. Adachi, Efficient persistent room temperature phosphorescence in organic amorphous materials under ambient conditions, *Adv. Funct. Mater.* 23 (2013) 3386–3397, <https://doi.org/10.1002/adfm.201203706>.
- [55] R. Kabe, C. Adachi, Organic long persistent luminescence, *Nature* 550 (2017) 384–387, <https://doi.org/10.1038/nature24010>.
- [56] I. Bhattacharjee, S. Hirata, Highly efficient persistent room-temperature phosphorescence from heavy atom-free molecules triggered by hidden long phosphorescent antenna, *Adv. Mater.* 32 (2020) 2001348, <https://doi.org/10.1002/adma.202001348>.
- [57] Y. Wang, J. Yang, M. Fang, Y. Yu, B. Zou, L. Wang, Y. Tian, J. Cheng, B.Z. Tang, Z. Li, Förster resonance energy transfer: an efficient way to develop stimulus-responsive room-temperature phosphorescence materials and their applications, *Matter* 3 (2020) 449–463, <https://doi.org/10.1016/j.matt.2020.05.005>.
- [58] Y. Zhang, Y. Su, H. Wu, Z. Wang, C. Wang, Y. Zheng, X. Zheng, L. Gao, Q. Zhou, Y. Yang, X. Chen, C. Yang, Y. Zhao, Large-area, flexible, transparent, and long-lived polymer-based phosphorescence films, *J. Am. Chem. Soc.* 143 (2021) 13675–13685, <https://doi.org/10.1021/jacs.1c05213>.
- [59] X. Wang, Y. Sun, G. Wang, J. Li, X. Li, K. Zhang, TADF-type organic afterglow, *Angew. Chem. Int. Ed.* 60 (2021) 17138–17147, <https://doi.org/10.1002/anie.202105628>.
- [60] M. Louis, H. Thomas, M. Gmelch, A. Ha, F. Fries, S. Reineke, Blue-light-absorbing thin films showing ultralong room-temperature phosphorescence, *Adv. Mater.* 31 (2019) 1807887, <https://doi.org/10.1002/adma.201807887>.
- [61] J. Jin, H. Jiang, Q. Yang, L. Tang, Y. Tao, Y. Li, R. Chen, C. Zheng, Q. Fan, K. Zhang, Q. Zhao, W. Huang, Thermally activated triplet exciton release for highly efficient tri-mode organic afterglow, *Nat. Commun.* 11 (2020) 842, <https://doi.org/10.1038/s41467-020-14669-3>.
- [62] Z. Yang, C. Xu, W. Li, Z. Mao, X. Ge, Q. Huang, H. Deng, J. Zhao, F. Gu, Y. Zhang, Z. Chi, Boosting the quantum efficiency of ultralong organic phosphorescence up to 52 % via intramolecular halogen bonding, *Angew. Chem. Int. Ed.* 59 (2020) 17451–17455, <https://doi.org/10.1002/anie.202007343>.
- [63] K. Jinnai, R. Kabe, Z. Lin, C. Adachi, Organic long-persistent luminescence stimulated by visible light in p-type systems based on organic photoredox catalyst dopants, *Nat. Mater.* 21 (2022) 338–344, <https://doi.org/10.1038/s41563-021-01150-9>.
- [64] W. Li, Z. Li, C. Si, M.Y. Wong, K. Jinnai, A.K. Gupta, R. Kabe, C. Adachi, W. Huang, E. Zysman-Colman, I.D.W. Samuel, Organic long-persistent luminescence from a thermally activated delayed fluorescence compound, *Adv. Mater.* 32 (2020) 2003911, <https://doi.org/10.1002/adma.202003911>.
- [65] J. Wang, Z. Huang, X. Ma, H. Tian, Visible-light-excited room-temperature phosphorescence in water by curcubit[8]uril-mediated supramolecular assembly, *Angew. Chem. Int. Ed.* 59 (2020) 9928–9933, <https://doi.org/10.1002/anie.201914513>.
- [66] Z. Zhang, Y. Chen, Y. Liu, Efficient room-temperature phosphorescence of a solid-state supramolecule enhanced by cucurbit[6]uril, *Angew. Chem. Int. Ed.* 58 (2019) 6028–6032, <https://doi.org/10.1002/anie.201901882>.
- [67] L. Bian, H. Shi, X. Wang, K. Ling, H. Ma, M. Li, Z. Cheng, C. Ma, S. Cai, Q. Wu, N. Gan, X. Xu, Z. An, W. Huang, Simultaneously enhancing efficiency and lifetime of ultralong organic phosphorescence materials by molecular self-assembly, *J. Am. Chem. Soc.* 140 (2018) 10734–10739, <https://doi.org/10.1021/jacs.8b03867>.
- [68] G. Wang, X. Chen, X. Li, Y. Zeng, K. Zhang, Mechanism landscape in pyrylium induced organic afterglow systems, *Chem. Sci.* 14 (2023) 8180–8186, <https://doi.org/10.1039/d3sc01500a>.
- [69] J. Wang, H. Zhang, L. Niu, X. Zhu, Y. Kang, R. Boulatov, Q. Yang, Organic composite crystal with persistent room-temperature luminescence above 650 nm by combining triplet–triplet energy transfer with thermally activated delayed fluorescence, *CCS Chem.* 2 (2020) 1391–1398, <https://doi.org/10.31635/ccschem.020.202000158>.
- [70] S. Kuila, S.J. George, Phosphorescence energy transfer: ambient afterglow fluorescence from water-processable and purely organic dyes via delayed sensitization, *Angew. Chem. Int. Ed.* 59 (59) (2020) 9393–9397, <https://doi.org/10.1002/anie.202002555>.
- [71] Q. Dang, Y. Jiang, J. Wang, J. Wang, Q. Zhang, M. Zhang, S. Luo, Y. Xie, K. Pu, Q. Li, Z. Li, Room-temperature phosphorescence resonance energy transfer for construction of near-infrared afterglow imaging agents, *Adv. Mater.* 32 (2020) 2006752, <https://doi.org/10.1002/adma.202006752>.
- [72] K. Jinnai, R. Kabe, C. Adachi, Wide-range tuning and enhancement of organic long-persistent luminescence using emitter dopants, *Adv. Mater.* 30 (2018) 1800365, <https://doi.org/10.1002/adma.201800365>.
- [73] S. Hirata, Recent advances in materials with room-temperature phosphorescence: photophysics for triplet exciton stabilization, *Adv. Opt. Mater.* 5 (2017) 1700116, <https://doi.org/10.1002/adom.201700116>.
- [74] S. Ding, Y. Xu, J. Li, X. Wang, G. Wang, H. Li, S. Ren, K. Zhang, Achieving long-lived room-temperature phosphorescence via charge transfer technology and dopant-matrix design strategy, *Dyes Pigments* 210 (2023) 110984, <https://doi.org/10.1016/j.dyepig.2022.110984>.
- [75] G. Wang, X. Li, X. Wang, K. Zhang, Efficient cascade reactions for luminescent pyrylium biolabels catalysed by light rare-earth elements, *New J. Chem.* 45 (2021) 12305–12310, <https://doi.org/10.1039/dnj01793d>.
- [76] J. Huang, X. Wang, G. Wang, J. Li, X. Deng, X. Chen, Y. Xu, C. Lei, K. Zhang, Polymer-based TADF-type organic afterglow, *J. Phys. Chem. C* 126 (2022) 20728–20738, <https://doi.org/10.1021/acs.jpcc.2c07499>.
- [77] J. Huang, X. Deng, J. Li, G. Wang, X. Li, H. Yao, C. Lei, K. Zhang, Developing robust organic afterglow emulsion for dissolved oxygen sensing, *Chem. Eng. J.* 474 (2023) 145809, <https://doi.org/10.1016/j.cej.2023.145809>.
- [78] J. Liu, Y. Sun, G. Wang, X. Chen, J. Li, X. Wang, Y. Zou, B. Wang, K. Zhang, Organic afterglow emulsions exhibiting 2.4 s phosphorescence lifetimes and specific protein binding property, *Adv. Opt. Mater.* 10 (2022) 2201502, <https://doi.org/10.1002/adom.202201502>.
- [79] A. Samanta, M. Höglund, P. Samanta, S. Popov, I. Sychugov, L. Maddalena, F. Carosio, L.A. Berglund, Charge regulated diffusion of silica nanoparticles into wood for flame retardant transparent wood, *Adv. Sustain. Syst.* 6 (2022) 2100354, <https://doi.org/10.1002/adss.202100354>.
- [80] M.L. Strugaru, S.G. Ţerban, A.M. Berdie, S. Jitian, Infrared spectra of the main optical properties of poly(methyl methacrylate) thin films, *Polym. Bull.* 81 (81) (2024) 11257–11271, <https://doi.org/10.1007/s0289-024-05242-9>.
- [81] E. Marimuthu, V. Murugesan, Influence of ultrasound on multi-site phase transfer catalyzed polymerization of N-vinyl carbazole in two phase system, *SN Appl. Sci.* 1 (2019) 638. <https://doi.org/10.1007/s42452-019-0661-7>.
- [82] C. Chen, Z. Chi, K.C. Chong, A.S. Batsanov, Z. Yang, Z. Mao, Z. Yang, B. Liu, Carbazole isomers induce ultralong organic phosphorescence, *Nat. Mater.* 20 (2021) 175–180, <https://doi.org/10.1038/s41563-020-0797-2>.
- [83] S. Xu, W. Wang, H. Li, J. Zhang, R. Chen, S. Wang, C. Zheng, G. Xing, C. Song, W. Huang, Design of highly efficient deep-blue organic afterglow through guest sensitization and matrices rigidification, *Nat. Commun.* 11 (2020) 4802. <https://doi.org/10.1038/s41467-020-18572-9>.

- [84] X. Li, X. Yue, Y. Wang, T. Chen, Y. Zhou, D. Liu, H. Xiang, S. Zhang, H. Zeng, Z. Xiang, Electron donor–acceptor (D-A) tuning to achieve soluble covalent organic polymers for optoelectronic devices, *eScience* 3 (2023) 100084. <https://doi.org/10.1016/j.esci.2022.10.009>.
- [85] Y. Lei, W. Dai, J. Guan, S. Guo, F. Ren, Y. Zhou, J. Shi, B. Tong, Z. Cai, J. Zheng, Y. Dong, Wide-range color-tunable organic phosphorescence materials for printable and writable security inks, *Angew. Chem. Int. Ed.* 59 (2020) 16054–16060. <https://doi.org/10.1002/anie.202003585>.
- [86] M. Pavlič, M. Petrić, J. Žigon, Interactions of coating and wood flooring surface system properties, *Coatings* 11 (2021) 91. <https://doi.org/10.3390/coatings11010091>.
- [87] L. Kong, D. Xu, Z. He, F. Wang, S. Gui, J. Fan, X. Pan, X. Dai, X. Dong, B. Liu, Y. Li, Nanocellulose-reinforced polyurethane for waterborne wood coating, *Molecules* 24 (2019) 3151. <https://doi.org/10.3390/molecules24173151>.
- [88] M.S. Ma'arif, R.T. Putri, K. Anam, Effect of bio-based adhesive on tensile strength and bending of balsa wood adhesive joint, *Int. J. Integr. Eng.* 11 (2019) 72–79. <https://doi.org/10.30880/ijie.2019.11.05.010>.
- [89] C.R. Westerman, B.C. McGill, J.J. Wilker, Sustainably sourced components to generate high-strength adhesives, *Nature* 621 (2023) 306–311. <https://doi.org/10.1038/s41586-023-06335-7>.
- [90] A. Kaymakci, Effect of titanium dioxide on some mechanical, thermal, and surface properties of wood-plastic nanocomposites, *BioResources* 14 (14) (2019) 1969–1979. <https://doi.org/10.15376/biores.14.1.1969-1979>.
- [91] N. Ayrilmis, M. Kariz, J.H. Kwon, M.K. Kuzman, Effect of printing layer thickness on water absorption and mechanical properties of 3D-printed wood/PLA composite materials, *Int. J. Adv. Manuf. Tech.* 102 (2019) 2195–2200. <https://doi.org/10.1007/s00170-019-03299-9>.
- [92] L. Liu, M. Lin, Z. Xu, M. Lin, Polylactic acid-based wood-plastic 3D printing composite and its properties, *BioResources* 14 (2019) 8484–8498. <https://doi.org/10.15376/biores.14.4.8484-8498>.
- [93] I. Romero-Ocaña, S.I. Molina, Cork photocurable resin composite for stereolithography (SLA): Influence of cork particle size on mechanical and thermal properties, *Addit. Manuf.* 51 (2022) 102586. <https://doi.org/10.1016/j.addma.2021.102586>.
- [94] S. Zhang, S. Bhagia, M. Li, X. Meng, A.J. Ragauskas, Wood-reinforced composites by stereolithography with the stress whitening behavior, *Mater. Design* 206 (2021) 109773. <https://doi.org/10.1016/j.matdes.2021.109773>.
- [95] X. Luo, B. Tian, Y. Zhai, H. Guo, S. Liu, J. Li, S. Li, T.D. James, Z. Chen, Room-temperature phosphorescent materials derived from natural resources, *Nat. Rev. Chem.* 7 (2023) 800–812. <https://doi.org/10.1038/s41570-023-00536-4>.
- [96] R. Rai, R. Ranjan, P. Dhar, Life cycle assessment of transparent wood production using emerging technologies and strategic scale-up framework, *Sci. Total Environ.* 846 (2022) 157301. <https://doi.org/10.1016/j.scitotenv.2022.157301>.